Journal of
Synchrotron
Radiation

ISSN 1600-5775

Received 1 November 2013
Accepted 8 May 2014

Theoretical consideration of an X-ray Bragg-reflection lens using the eikonal approximation

Minas K. Balyan

Faculty of Physics, Department of Solid State Physics, Yerevan State University, Alex Manoogian 1, Yerevan 0025, Armenia. E-mail: mbalyan@ysu.am

On the basis of the eikonal approximation, X-ray Bragg-case focusing by a perfect crystal with parabolic-shaped entrance surface is considered theoretically. Expressions for focal distances, intensity gain and distribution around the focus spot as well as for the focus spot sizes are obtained. The condition of point focusing is presented. The experiment can be performed using X-ray synchrotron radiation sources (particularly free-electron lasers).

Keywords: eikonal approximation; Bragg reflection; X-ray point focusing; X-ray lens.

1. Introduction

The focusing of a diffracted X-ray beam may be achieved using a perfect crystal with parabolic-shaped surface. Theoretical and experimental investigations of sagittal focusing in the Bragg case by such a crystal has been carried out by Hrdý (1998), Hrdý *et al.* (2001*a*), Hrdý & Siddons (1999) and Artemiev *et al.* (2001). Meridional focusing in the Bragg case has been investigated by Hrdý & Hrdá (2000) and Hrdý *et al.* (2001*b*), and Laue-case focusing was considered by Hrdý *et al.* (2003). In these works the plane-wave dynamical diffraction theory is used, and the focusing distance was determined. The determination of other important parameters, *i.e.* the focus spot size, intensity gain and intensity distribution around the focus spot, require the use of the dynamical diffraction theory for a spatially inhomogeneous X-ray beam. Takagi's equations (Takagi, 1969) describe the diffraction of a spatially inhomogeneous X-ray wave depending only on the coordinates of an observation point in the diffraction plane (usually x and z); the coordinate perpendicular to the diffraction plane (the coordinate y) is a parameter. However, in the case of focusing by a perfect crystal with parabolic-shaped surface, the y coordinate cannot be set as a parameter. It has the meaning of an essential coordinate (as x and z). Therefore, one needs to improve Takagi's equations by taking into account the coordinate y. It is clear that the wave-optical consideration of the two-dimensional focusing phenomena based on such equations will be complicated. However, the main purpose of focusing is to obtain an image of a point source. Since a point source emits a spherical wave, which, after reflection by a focusing element, gives rise to secondary emitted spherical waves, the problem can be effectively solved using trajectory methods or the so-called eikonal approximation. This means that the emitted as well as the secondary emitted spherical waves can be presented as locally plane waves varying across the wavefront wavevectors (Solimeno *et al.*, 1986). The gradient of the eikonal function at an arbitrary point of the wavefront gives the corresponding wavevector. The eikonal approximation of Takagi's equations is considered by Chukhovskii & Shtolberg (1970) and Kohn (2007), and in textbooks by Authier (2001) and Pinsker (1982). Further development of the eikonal approximation, taking into account two-dimensional curvature of the wavefront, is given by Balyan (2013*a*). Balyan (2013*b*) applies this theory for investigation of Laue-case focusing by a perfect crystal with parabolic-shaped surface.

In this work, the eikonal approximation is used for theoretical investigation of X-ray Bragg-case focusing by a perfect crystal with parabolic-shaped entrance surface (the crystal is not bent). First, however, in the following section, the general formulae, given by Balyan (2013*a*), are discussed and adopted for Bragg-case diffraction.

2. Eikonal and trajectories in the Bragg case

In the Bragg case it is convenient to take the axis Oz directed inward to the crystal and the axis Ox towards the entrance surface in the diffraction plane (Fig. 1). The axis Oy is perpendicular to the diffraction plane (x, z). In Fig. 1, a Bragg-case perfect crystal with parabolic-shaped entrance surface is shown with its reflecting planes. The reflecting planes are not curved. The case of an elastically bent crystal here is not considered. In Fig. 1, incident as well as reflected rays are shown.

2.1. Eikonal equations inside a perfect crystal and in vacuum in the case of two-dimensional curvature of the wavefront

In the case of two-wave dynamical diffraction the wavefield in a perfect crystal for any polarization state is given in the form

$$E = \left[\tilde{E}_0 \exp(i\mathbf{K}_0\mathbf{r}) + \tilde{E}_h \exp(i\mathbf{K}_h\mathbf{r})\right] \exp(ik\chi_0 x/2\cos\theta). \quad (1)$$

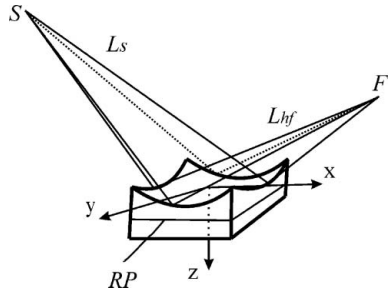

Figure 1
X-ray focusing scheme in the Bragg case using a parabolic-shaped entrance-surface perfect crystal. *S*, X-ray point source; *F*, point focus; RP, reflecting planes; for other notations see text.

where $\mathbf{K}_0$ is the wavevector of the transmitted wave, $\mathbf{K}_h = \mathbf{K}_0 + \mathbf{h}$ is the wavevector of the diffracted wave, $\mathbf{h}$ is the diffraction vector, $\mathbf{K}_0^2 = \mathbf{K}_h^2 = k^2 = (2\pi/\lambda)^2$, λ is the wavelength in a vacuum, χ_0 is the zero-order Fourier component of the crystal susceptibility, χ_h and $\chi_{\bar{h}}$ [see below, equation (2)] are the Fourier coefficients of the crystal susceptibility for the reciprocal lattice vectors $\mathbf{h}$ and $-\mathbf{h}$, respectively, θ is the Bragg angle, and $\tilde{E}_0$ and $\tilde{E}_h$ are the amplitudes of the transmitted and diffracted waves, respectively. In the case of two-dimensional curvature of the wavefront, taking into account the second derivatives with respect to the coordinate y, one can obtain the following dynamical diffraction equations in a perfect crystal (Balyan, 2013*a*, and references therein),

$$\begin{aligned}\partial^2\tilde{E}_0/\partial y^2 + 2ik\partial\tilde{E}_0/\partial s_0 + k^2\chi_{\bar{h}}\tilde{E}_h C = 0,\\ \partial^2\tilde{E}_h/\partial y^2 + 2ik\partial\tilde{E}_h/\partial s_h + k^2\chi_h\tilde{E}_0 C = 0,\end{aligned} \tag{2}$$

where $s_0 = (x/\cos\theta + z/\sin\theta)/2$ and $s_h = (x/\cos\theta - z/\sin\theta)/2$ are the coordinates along the transmitted and diffracted waves, respectively, C is the polarization factor equal to 1 for σ-polarization and to $\cos 2\theta$ for π-polarization. Hereafter, C is set as equal to 1. For separate amplitudes from (2) one finds the following dynamical diffraction equations,

$$\frac{\partial^4\tilde{E}_{0,h}}{\partial y^4} + 2ik\left(\frac{\partial}{\partial s_0} + \frac{\partial}{\partial s_h}\right)\frac{\partial^2\tilde{E}_{0,h}}{\partial y^2} - 4k^2\frac{\partial^2\tilde{E}_{0,h}}{\partial s_0\partial s_h} - k^4\chi_h\chi_{\bar{h}}\tilde{E}_{0,h} = 0. \tag{3}$$

The eikonal approximation for amplitudes has the form

$$\tilde{E}_{0,h} = E_{0,h}\exp(i\Phi), \tag{4}$$

where Φ is the eikonal and $E_{0,h}$ are slowly varying amplitudes. The eikonal equation is obtained by substituting expression (4) into (3) and neglecting the derivatives of amplitudes and higher-order derivatives of the eikonal,

$$\left(\Phi_y^2 + 2k\cos\theta\,\Phi_x\right)^2 - 4k^2\Phi_z^2\sin^2\theta - k^4\chi_h\chi_{\bar{h}} = 0. \tag{5}$$

Here a subscript of the eikonal means differentiation with respect to the corresponding variable.

Inserting (4) into the system (2) and neglecting the derivatives of amplitudes and higher-order derivatives of the eikonal, one can find the relation between the amplitudes,

$$E_h = \frac{2E_0\left[(1/2k)\Phi_y^2 + (\cos\theta\,\Phi_x + \sin\theta\,\Phi_z)\right]}{k\chi_{\bar{h}}}. \tag{6}$$

In a vacuum the reflected wave has the form $\tilde{E}_h^{(e)}\exp(i\mathbf{K}_h\mathbf{r})$ with slowly varying amplitude $\tilde{E}_h^{(e)}$ which satisfies the parabolic equation of diffraction (Grigoryan *et.al.*, 2010),

$$\frac{1}{\sin^2\theta}\frac{\partial^2\tilde{E}_h^{(e)}}{\partial x^2} + \frac{\partial^2\tilde{E}_h^{(e)}}{\partial y^2} + 2ik\left(\cos\theta\frac{\partial}{\partial x} - \sin\theta\frac{\partial}{\partial z}\right)\tilde{E}_h^{(e)} = 0. \tag{7}$$

Here the superscript (e) means external. Representing $\tilde{E}_h^{(e)} = E_h^{(e)}\exp[i\Phi^{(e)}]$, substituting into (7) and neglecting the derivatives of amplitude $E_h^{(e)}$ and higher-order derivatives of the eikonal one can find the eikonal equation in a vacuum,

$$\frac{1}{\sin^2\theta}\Phi_x^{(e)2} + \Phi_y^{(e)2} + 2k\left[\cos\theta\,\Phi_x^{(e)} - \sin\theta\,\Phi_z^{(e)}\right] = 0. \tag{8}$$

2.2. The complete integral and solutions of eikonal equations

The complete integral of a first-order partial differential equation of three variables is the solution $\Phi(x, y, z, C_1, C_2, C_3)$ depending on three arbitrary constants C_1, C_2, C_3. The complete integral is used for solving first-order partial differential equations. In our case it can be used for solving the eikonal equations (5) and (8). The standard procedure is as follows (Smirnov, 1981; Courant & Hilbert, 1966). Let the entrance surface of the crystal be given parametrically by

$$x = x(t_1, t_2), \qquad y = y(t_1, t_2), \qquad z = z(t_1, t_2). \tag{9}$$

The eikonal on the entrance surface is a known function $\Phi_0(t_1, t_2)$. From the continuity conditions,

$$\begin{aligned}\Phi_0(t_1, t_2) &= \Phi\left[x(t_1, t_2), y(t_1, t_2), z(t_1, t_2), C_1, C_2, C_3\right],\\ \Phi_{0t_1} &= \Phi_{t_1},\\ \Phi_{0t_2} &= \Phi_{t_2}.\end{aligned} \tag{10}$$

From (10) the constants C_1, C_2 and C_3 are defined as functions depending on t_1 and t_2. Inserting these functions into the expression of the complete integral one finds the so-called general integral $\Phi[x, y, z, C_1(t_1, t_2), C_2(t_1, t_2), C_3(t_1, t_2)]$. The general integral depends on two arbitrary parameters, t_1 and t_2. From the set

$$\begin{aligned}\Phi_{t_1}[x, y, z, C_1(t_1, t_2), C_2(t_1, t_2), C_3(t_1, t_2)] = 0,\\ \Phi_{t_2}[x, y, z, C_1(t_1, t_2), C_2(t_1, t_2), C_3(t_1, t_2)] = 0,\end{aligned} \tag{11}$$

the parameters t_1 and t_2 can be defined as functions on (x, y, z). Inserting these functions into the expression of the general integral one finds the eikonal satisfying the given boundary conditions. The set (11) defines a trajectory, passing through the points with coordinates $[x(t_1, t_2), y(t_1, t_2), z(t_1, t_2)]$ (on the entrance surface) and (x, y, z) (inside the crystal). The general integral is the eikonal on the trajectory for a given pair (t_1, t_2). From (11) it follows that on this trajectory with fixed (x, y, z) for arbitrary variations of δt_1 and δt_2 the variation of the eikonal $\delta\Phi = \Phi_{t_1}\delta t_1 + \Phi_{t_2}\delta t_2 = 0$, *i.e.* on a trajectory the eikonal has an extremum.

3. Complete integrals inside a perfect crystal and in a vacuum

The complete integrals of eikonal equations (5) and (8) can be found by the method of variable separation. The solution is presented in the form

$$\Phi = \Phi_1(x) + \Phi_2(y) + \Phi_3(z). \tag{12}$$

Inserting (12) into (5) and (8) it is easy to find the following complete integrals. For the complete integral inside a crystal we have two solutions,

$$\Phi^{(\pm)} = \pm z\left[A_1^{(\pm)2}\cos^2\theta - \sigma^2\right]^{1/2}/\sin\theta + A_2^{(\pm)}y + A_1^{(\pm)}x - A_2^{(\pm)2}x/2k\cos\theta + A_3^{(\pm)}, \tag{13}$$

and for the complete integral in a vacuum

$$\Phi^{(e)} = C_1(x + z\cot\theta) + C_2 y + C_1^2 z/(2k\sin^3\theta) + C_2^2 z/(2k\sin\theta) + C_3, \tag{14}$$

where A_1, A_2 and A_3, C_1, C_2 and C_3 are arbitrary constants and $\sigma = k(\chi_h\chi_{\bar{h}})^{1/2}/2$. The signs '$\pm$' on the left-hand side of (13) correspond to the '$\pm$' signs on the right-hand side.

4. Continuity conditions

A spatially inhomogeneous incident wave can be presented in the form $E_0^{(i)}\exp[i\Phi^{(i)}]\exp[i\mathbf{K}_0^{(i)}\mathbf{r}]$, where $E_0^{(i)}$ is the slowly varying amplitude, $\Phi^{(i)}$ is the eikonal, $\mathbf{K}_0^{(i)}$ is the carrying wavevector and $\mathbf{r}$ is the radius vector of an observation point. Here the superscript '(i)' means 'incident'. For the Bragg-case diffraction the following continuity condition on the entrance surface of the crystal can be written [see (1)]

$$E_0^{(i)}\exp\left[i\Phi^{(i)}\right]\exp\left[i\mathbf{K}_0^{(i)}\mathbf{r}_0\right] = \left\{E_{01}\exp\left[i\Phi^{(1)}\right] + E_{02}\exp\left[i\Phi^{(2)}\right]\right\} \times \exp(ik\chi_0 x_0/2\cos\theta)\exp(i\mathbf{K}_0\mathbf{r}_0), \tag{15}$$

where $\mathbf{r}_0$ is the radius vector of an arbitrary point of the entrance surface. $\Phi^{(1)}$ and $\Phi^{(2)}$ are eikonals and E_{01}, E_{02} are the amplitudes corresponding to two solutions of the eikonal (5). Since E_{01} and E_{02} are slowly varying functions as $E_0^{(i)}$, and $\exp[i\Phi^{(1)}]$, $\exp[i\Phi^{(2)}]$ have the same order of variation as $\exp[i\Phi^{(i)}]$, from (15) one can write

$$E_0^{(i)} = E_{01} + E_{02}, \tag{16}$$

$$\Phi^{(i)} + \left[\mathbf{K}_0^{(i)} - \mathbf{K}_0\right]\mathbf{r}_0 = \Phi^{(1)} + k\chi_0 x_0/2\cos\theta = \Phi^{(2)} + k\chi_0 x_0/2\cos\theta. \tag{17}$$

For the reflected wave one can write the following continuity conditions,

$$E_{h1} + E_{h2} = E_h^{(e)},$$

$$\Phi^{(i)} + \left[\mathbf{K}_0^{(i)} - \mathbf{K}_0\right]\mathbf{r}_0 = \Phi^{(1)} + k\chi_0 x_0/2\cos\theta = \Phi^{(2)} + k\chi_0 x_0/2\cos\theta = \Phi^{(e)}. \tag{18}$$

5. Solution of the eikonal equation inside the crystal and amplitudes

The entrance surface of the crystal has parabolic form with the radius of curvature $R_{x,y}$ at the apex (Fig. 1) and is given by the equation

$$z_0 = x_0^2/2R_x + y_0^2/2R_y. \tag{19}$$

Let us consider an X-ray point source S placed at a distance L_s from the apex of the groove (the origin O of the coordinate system) (Fig. 2). The line SO is the central ray impinging the crystal at the origin. The glancing angle between SO and reflecting planes is $\theta^{(i)}$. The source has a radius vector $\mathbf{r}_s$ with coordinates $x_s = -L_s\cos\theta^{(i)}$, $y_s = 0$, $z_s = -L_s\sin\theta^{(i)}$. Let us denote the deviation angle of the central ray from the Bragg exact direction by $\Delta\theta = \theta^{(i)} - \theta$ (Fig. 2). The point source emits a spherical wave $\exp(ik|\mathbf{r} - \mathbf{r}_s|)/|\mathbf{r} - \mathbf{r}_s|$, where $\mathbf{r}$ is the radius vector of an arbitrary observation point. For the entrance surface of the crystal we have $\exp(ik|\mathbf{r}_0 - \mathbf{r}_s|)/|\mathbf{r}_0 - \mathbf{r}_s|$. In the denominator with high accuracy one can take $|\mathbf{r} - \mathbf{r}_s| \simeq L_s$. We expand the argument of the exponential into the Taylor series with accuracy including quadratic terms, *i.e.*

$$\begin{aligned} k|\mathbf{r}_0 - \mathbf{r}_s| &= k\left[(x_0 - x_s)^2 + (y_0 - y_s)^2 + (z_0 - z_s)^2\right]^{1/2} \\ &\simeq k\left[L_s + x_0\cos\theta^{(i)} + z_0\sin\theta^{(i)} + \left(x_0^2\sin^2\theta + y_0^2 + z_0^2\cos^2\theta\right)/(2L_s)\right] \\ &= kL_s + \mathbf{K}_0^{(i)}\mathbf{r}_0 + k\left(x_0^2\sin^2\theta + y_0^2 + z_0^2\cos^2\theta\right)/(2L_s). \end{aligned} \tag{20}$$

According to (20), $E_0^{(i)} = \exp(ikL_s)/L_s$, $\Phi^{(i)} = k(x_0^2\sin^2\theta + y_0^2 + z_0^2\cos^2\theta)/(2L_s)$, the carrying wavevector $\mathbf{K}_0^{(i)}$ has components $K_{0x}^{(i)} = k\cos\theta^{(i)}$, $K_{0y}^{(i)} = 0$, $K_{0z}^{(i)} = k\sin\theta^{(i)}$. In the quadratic terms we take θ instead of $\theta^{(i)}$ since $\Delta\theta$ is the order of a few arc-

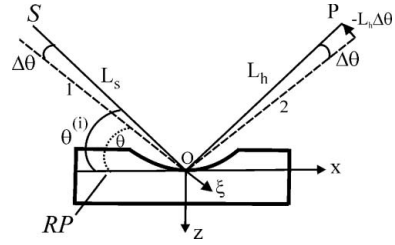

Figure 2
Scheme of reflection in the plane (x, z) $(y = 0)$. SO, central incident ray; OP, central reflected ray; $\theta^{(i)}$, glancing angle between central ray SO and reflecting planes RP; the glancing angle between the central reflected ray OP and the reflecting planes is also $\theta^{(i)}$; 1 and 2, lines parallel to the exact Bragg directions of the incident and reflected waves, respectively; $\Delta\theta = \theta^{(i)} - \theta$; $O\xi$, axis of the ξ coordinate perpendicular to the direction of line 2; $-L_h\Delta\theta$ is the ξ coordinate of an arbitrary point on the central ray PO at a distance L_h.

seconds. $\mathbf{K}_0$ [see (1)] has components $K_{0x} = k\cos\theta$, $K_{0y} = 0$, $K_{0z} = k\sin\theta$. According to (19) and (20),

$$\Phi^{(i)} = k\frac{x_0^2\sin^2\theta}{2L_s}\left[1+\left(\frac{x_0}{2R_x\tan\theta}\right)^2+\frac{y_0^2}{4R_xR_y\tan^2\theta}\right] + k\frac{y_0^2}{2L_s}\left[1+\left(\frac{y_0\cos\theta}{2R_y}\right)^2+\frac{x_0^2\cos^2\theta}{4R_xR_y\tan^2\theta}\right]. \quad (21)$$

We are interested in the region near the apex of the groove where $|x_0/R_{x,y}| < 1$ and $|y_0/R_{x,y}| < 1$. In the case of sufficiently large L_s, particularly for the case of a plane incident wave, the second and the third terms in the brackets of (21) are small. After neglecting these terms,

$$\Phi^{(i)} = k\frac{x_0^2\sin^2\theta}{2L_s}+k\frac{y_0^2}{2L_s}. \quad (22)$$

Now the continuity conditions (10) for a transmitted wave, taking into account (13), (17), (19) and (22), take the form ($t_1 = x_0$, $t_2 = y_0$)

$$\begin{aligned}
&-\sigma_0x_0+k\cos\theta\Delta\theta z_0+k\frac{x_0^2\sin^2\theta}{2L_s}+k\frac{y_0^2}{2L_s} = \\
&\qquad \pm z_0\left[A_1^{(\pm)2}\cos^2\theta-\sigma^2\right]^{1/2}/\sin\theta+A_1^{(\pm)}x_0 \\
&\qquad -A_2^{(\pm)2}x_0/2k\cos\theta+A_2^{(\pm)}y_0+A_3^{(\pm)}, \\
&Q_1x_0-\sigma_0 = \pm\frac{x_0}{R_x}\left[A_1^{(\pm)2}\cos^2\theta-\sigma^2\right]^{1/2}/\sin\theta+A_1^{(\pm)} \\
&\qquad -A_2^{(\pm)2}/2k\cos\theta, \quad (23)\\
&Q_2y_0 = \pm\frac{y_0}{R_y}\left[A_1^{(\pm)2}\cos^2\theta-\sigma^2\right]^{1/2}/\sin\theta+A_2^{(\pm)},
\end{aligned}$$

where

$$\begin{aligned}
\sigma_0 &= k\sin\theta(\Delta\theta+\chi_0/\sin2\theta),\\
Q_1 &= k\sin\theta\left(\frac{\sin\theta}{L_s}+\frac{\Delta\theta}{R_x\tan\theta}\right), \quad (24)\\
Q_2 &= k\left(\frac{1}{L_s}+\frac{\cos\theta\Delta\theta}{R_y}\right).
\end{aligned}$$

According to the third equation of (23), A_2 is linear on y_0 and in (23) the term A_2^2 is quadratic on y_0 and can be neglected. Solving the system (23) one finds the following solutions,

$$\begin{aligned}
A_1^{(\pm)} &= \Bigg((Q_1x_0-\sigma_0)\cos\theta\mp[x_0/(R_x\tan\theta)] \\
&\quad\times\left\{(Q_1x_0-\sigma_0)^2\cos^2\theta-\sigma^2\left[1-x_0^2/\left(R_x^2\tan^2\theta\right)\right]\right\}^{1/2}\Bigg) \\
&\quad\Big/\left\{\cos\theta\left[1-x_0^2/\left(R_x^2\tan^2\theta\right)\right]\right\},\\
A_2^{(\pm)} &= -Q_\pm^{(y)}y_0,\\
A_3^{(\pm)} &= \frac{Q_\pm^{(x)}x_0^2}{2}+\frac{Q_\pm^{(y)}y_0^2}{2}, \quad (25)
\end{aligned}$$

where

$$\begin{aligned}
Q_\pm^{(x)} &= \left\{\pm\frac{\left[A_1^{(\pm)2}\cos^2\theta-\sigma^2\right]^{1/2}}{R_x\sin\theta}-Q_1\right\},\\
Q_\pm^{(y)} &= \left\{\pm\frac{\left[A_1^{(\pm)2}\cos^2\theta-\sigma^2\right]^{1/2}}{R_x\sin\theta}-Q_2\right\}. \quad (26)
\end{aligned}$$

Here the signs correspond to the signs in the complete integral expression (13). Inserting the obtained $A_{1,2,3}$ into (13) we find the general integral (the term with A_2^2 is neglected). The trajectories are obtained using the set (11) ($t_1 = x_0$, $t_2 = y_0$),

$$\begin{aligned}
&\pm\frac{A_1^{(\pm)}\cos^2\theta A_{1x_0}^{(\pm)}}{\sin\theta\left[A_1^{(\pm)2}\cos^2\theta-\sigma^2\right]^{1/2}}\left[z-\frac{x_0}{R_x}(x-x_0/2)\right. \\
&\qquad\left.-\frac{y_0}{R_y}(y-y_0/2)\right]+Q_\pm^{(x)}(x_0-x)=0,\\
&Q_\pm^{(y)}(y_0-y)=0. \quad (27)
\end{aligned}$$

From the second equation of (27), $y_0 = y$. Near the entrance surface of the crystal, where $z \simeq x^2/(2R_x)+y^2/(2R_y) = z_0(x,y)$, from the first equation of (27) we have $x_0 \simeq x$. Inserting the obtained x_0 and y_0 into the general integral $\Phi^{(\pm)}[x, y, z, A_1^{(\pm)}(x_0, y_0), A_2^{(\pm)}(x_0, y_0), A_3^{(\pm)}(x_0, y_0)]$, one finds the eikonal near the entrance surface of the crystal,

$$\begin{aligned}
\Phi^{(1,2)} = &\pm\frac{\left[A_1^{(\pm)2}\cos^2\theta-\sigma^2\right]^{1/2}}{\sin\theta}\left[z-z_0(x,y)\right]+\frac{Q_1x^2}{2}\\
&+\frac{Q_2y^2}{2}-\sigma_0x. \quad (28)
\end{aligned}$$

Here the superscript 1 corresponds to the '+' sign on the right-hand side and the superscript 2 corresponds to the '−' sign. Using (28) and (6) (neglecting Φ_y^2) one finds the amplitude of the diffracted wave on the entrance surface $z = z_0(x, y)$,

$$E_{h(1,2)} = \frac{2E_{0(1,2)}}{k\chi_{\bar{h}}}\left\{A_1^{(\pm)}\cos\theta\pm\left[A_1^{(\pm)2}\cos^2\theta-\sigma^2\right]^{1/2}\right\}. \quad (29)$$

From the second equation of (23) and the first equation of (25),

$$\begin{aligned}
&\pm\left[A_1^{(\pm)2}\cos^2\theta-\sigma^2\right]^{1/2} = \\
&\quad\Bigg(-(Q_1x-\sigma_0)\cos\theta\frac{x}{R_x\tan\theta}\pm\Big\{(Q_1x-\sigma_0)^2\cos^2\theta\\
&\qquad-\sigma^2\left[1-x^2/\left(R_x^2\tan^2\theta\right)\right]\Big\}^{1/2}\Bigg)\Big/\left[1-x^2/\left(R_x^2\tan^2\theta\right)\right]. \quad (30)
\end{aligned}$$

As can be seen from (28) and (30), in the region where the argument of the square root of the right-hand side of (30) has a negative real part, only the solution with the '+' sign must be taken. This region corresponds to the total reflection region for a plane entrance surface crystal. Hereafter we will call this region the 'reflection region'. According to (30), in this region

$$(Q_1 x - \sigma_{0r})^2 \cos^2\theta < \sigma_r^2\left[1 - x^2/\left(R_x^2 \tan^2\theta\right)\right]. \quad (31)$$

Here σ_{0r} and σ_r are the real parts of the corresponding quantities. Taking into account the definition of σ_0 [see (24)] one can put $\sigma_{0r} = 0$ and $\Delta\theta = |\chi_{0r}|/\sin 2\theta$. For a crystal with a plane entrance surface this corresponds to the middle point of the total reflection region for the central incident ray SO (Fig. 2). From (31),

$$|x| < \frac{\sigma_r}{\left[Q_1^2 \cos^2\theta + \sigma_r^2/(R_x^2 \tan^2\theta)\right]^{1/2}} \equiv a_x. \quad (32)$$

For $|R_x| \to \infty$ (crystal with a flat entrance surface),

$$a_x \sin\theta = L_s |\chi_{hr}|/\sin 2\theta, \quad (33)$$

and, for $L_s \to \infty$ (plane incident wave),

$$a_x = |R_x| \tan\theta \frac{|\chi_{hr}|}{\left(|\chi_{0r}|^2 + |\chi_{hr}|^2\right)^{1/2}}. \quad (34)$$

For definiteness, without loss of generality, let us consider the case of a concave surface, *i.e.* $R_{x,y} < 0$. In the reflection region $-a_x \le x \le a_x$ the eikonal $\Phi = \Phi^{(1)}$, $E_{01} = E_0^{(i)}$, $E_{02} = 0$, E_{h1} is given by (29) and $E_{h2} = 0$. In the region $a_x \le x \le |R_x| \tan\theta$ and for $Q_1 < 0$ (particularly for the case of an incident plane wave) the same solution must be taken [since the absolute value of the corresponding amplitude decreases, see (35) below]. In the region $-|R_x| \tan\theta \le x \le -a_x$ we have $\Phi = \Phi^{(2)}$, $E_{02} = E_0^{(i)}$, $E_{01} = 0$, E_{h2} is given by (29) and $E_{h1} = 0$. For the case $Q_1 > 0$, $\Phi = \Phi^{(1)}$ in the reflection region and in the region $-|R_x| \tan\theta \le x \le -a_x$, and $\Phi = \Phi^{(2)}$ in the region $a_x \le x \le |R_x| \tan\theta$. At the point $x = -|R_x| \tan\theta$ the incident-beam central ray propagation direction is almost parallel to the entrance surface, the specular reflected waves must be taken into account and the presented formulae near this point are not valid. In the region $x < -|R_x| \tan\theta$ the mixed Laue–Bragg case is realised. Similarly, at the point $x = |R_x| \tan\theta$ the reflected-beam central ray propagation direction is almost parallel to the entrance surface and the presented formulae near this point are also not valid. In the region $x > |R_x| \tan\theta$ the mixed Bragg–Laue case is realised. Thus, for $Q_1 < 0$ in the region $-a_x \le x < |R_x| \tan\theta$,

$$E_h = E_{h1} = \Big(2E_0^{(i)}\Big\{(Q_1 x - \sigma_0)\cos\theta + \left[(Q_1 x - \sigma_0)^2 \cos^2\theta - \sigma^2\left(1 - x^2/R_x^2 \tan^2\theta\right)\right]^{1/2}\Big\}\Big) \Big/ \left[k\chi_{\bar{h}}(1 + x/R_x \tan\theta)\right], \quad (35)$$

and, in the region $-|R_x| \tan\theta < x \le -a_x$,

$$E_h = E_{h2} = \Big(2E_0^{(i)}\Big\{(Q_1 x - \sigma_0)\cos\theta - \left[(Q_1 x - \sigma_0)^2 \cos^2\theta - \sigma^2\left(1 - x^2/R_x^2 \tan^2\theta\right)\right]^{2}\Big\}\Big) \Big/ \left[k\chi_{\bar{h}}(1 + x/R_x \tan\theta)\right]. \quad (36)$$

For $Q_1 > 0$, $E_h = E_{h2}$ in (35) and $E_h = E_{h1}$ in (36) must be taken. The corresponding reflection coefficient

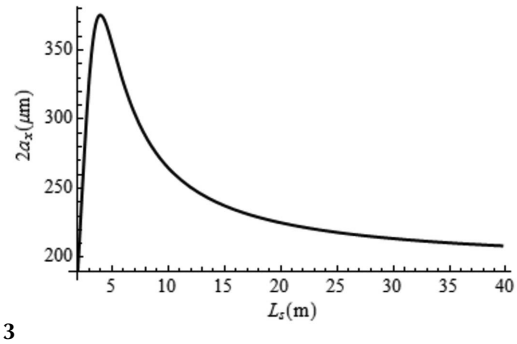

Figure 3
Dependence of the reflection region size on L_s.

$$R(x) = \left|E_h(x)/E_0^{(i)}\right|^2 \sin[\theta + \alpha(x)]/\sin[\theta - \alpha(x)] \quad (37)$$

can be calculated. Here $\tan\alpha(x) = x/R_x$. Below (in §8, Fig. 3), an example of $R(x)$ will be presented.

6. Focusing in a vacuum and focusing distance

According to (28), on the entrance surface of the crystal $z = z_0(x, y)$,

$$\Phi^{(1,2)} = \frac{Q_1 x^2}{2} + \frac{Q_2 y^2}{2} - \sigma_0 x. \quad (38)$$

According to (18), on the entrance surface,

$$\Phi^{(e)}(x, y) \equiv \Phi^{(e)}[x, y, z = z_0(x, y)] = \frac{Q_1 x^2}{2} + \frac{Q_2 y^2}{2} - kx \sin\theta \Delta\theta. \quad (39)$$

Using the Huygens–Fresnel principle for a curved surface (Grigoryan *et al.*, 2010) and the corresponding Green function in a vacuum in the parabolic approximation (Fresnel propagator) for the amplitude $\tilde{E}_h^{(e)}$ in a vacuum at an observation point (x, y, z), one can write the following approximate expression,

$$\tilde{E}_h^{(e)} = -\frac{ik \sin\theta}{2\pi L_h} \int_{-a_x}^{a_x} dx' \int_{-|R_y|}^{|R_y|} dy'\, E_{h1}(x') \exp\Big\{ik\big[(\xi - \xi')^2/(2L_h) + (y - y')^2/(2L_h)\big] + i\Phi^{(e)}(x', y')\Big\}, \quad (40)$$

where x', y' are the coordinates of an arbitrary point on the entrance surface of the crystal, $\xi' = x' \sin\theta + z_0(x', y') \cos\theta$, $\xi = x \sin\theta + z \cos\theta$ is the coordinate across the diffracted beam in the diffraction plane (Fig. 2), $L_h = -z/\sin\theta > 0$ is the crystal-to-observation point distance along the propagation direction of the diffracted beam, the line $\xi = 0$ is parallel to the exact Bragg direction of the reflected beam and the line $\xi = -L_h \Delta\theta$ is the central ray OP of the reflected wave (Fig. 2). The region of integration, for simplicity, we take in the form of the rectangle $[-a_x, a_x] \times [-|R_y|, |R_y|]$. The term $k\xi'^2/(2L_h)$ in the phase of the integrand with the accuracy of quadratic terms can be taken as $kx'^2 \sin^2\theta/(2L_h)$. In the phase of the integrand, combining the terms $-k\xi z_0(x', y') \cos\theta/L_h$ and

$Q_1 x'^2/2 + Q_2 y'^2/2$, taking in these terms $\xi = -L_h \Delta\theta$ (with the accuracy of quadratic terms), (40) can be rewritten in the form

$$\tilde{E}_h^{(e)} = -\frac{ik \sin\theta}{2\pi L_h} \int\limits_{-a_x}^{a_x} dx' \int\limits_{-|R_y|}^{|R_y|} dy' \; E_{h1}(x') \exp[i\Omega(\xi, \xi'', y, y'')], \tag{41}$$

where $\xi'' = x' \sin\theta$,

$$\begin{aligned} \Omega(\xi, \xi'', y, y') &= k(\xi - \xi'')^2/(2L_h) + k(y - y')^2/(2L_h) \\ &\quad + \Phi_0^{(e)}(\xi'', y'), \\ \Phi_0^{(e)}(\xi'', y') &= kA\xi''^2/(2\sin\theta) + kBy'^2/2 - k\xi''\Delta\theta, \\ A &= \sin\theta/L_s + 2\cot\theta\Delta\theta/R_x, \\ B &= 1/L_s + 2\cos\theta\Delta\theta/R_y. \end{aligned} \tag{42}$$

According to the stationary phase method the trajectories are obtained by differentiation of the phase of the integrand with respect to the integration variables and setting them equal to zero,

$$\begin{aligned} \xi''\left(\frac{\sin\theta}{L_h} + A\right) - \left(\frac{\xi}{L_h} + \Delta\theta\right)\sin\theta = 0, \\ y'\left(\frac{1}{L_h} + B\right) - \frac{y}{L_h} = 0. \end{aligned} \tag{43}$$

As can be seen from (43), the trajectories are straight lines which in the plane (ξ, L_h) are intersected at the point with the coordinates (ξ_f, L_{hfx}) (meridional focusing) and in the plane (y, L_h) are intersected at the point with the coordinates (y_f, L_{hfy}) (sagittal focusing). The coordinates of the focus points satisfy the relations

$$\begin{aligned} 1/L_s + 1/L_{hfx} &= 1/F_x, \\ \xi_f &= -L_{hfx}\Delta\theta, \end{aligned} \tag{44}$$

and

$$\begin{aligned} 1/L_s + 1/L_{hfy} &= 1/F_y, \\ y_f &= 0. \end{aligned} \tag{45}$$

Here the focal distances $F_{x,y}$ are determined as

$$\begin{aligned} F_x &= -R_x \sin\theta/(2\cot\theta\Delta\theta), \\ F_y &= -R_y/(2\cos\theta\Delta\theta). \end{aligned} \tag{46}$$

Since in the reflection region at the apex of the groove $\Delta\theta > 0$ (for central incident ray SO; Fig. 2), then for the focusing in both directions it should be $R_{x,y} < 0$, *i.e.* the groove must have a concave form. For the middle point of the reflection region for a crystal with a plane entrance surface, $\Delta\theta = |\chi_{0r}|/\sin 2\theta$ [see (31)] (Authier, 2001; Pinsker, 1982), and in this important case

$$\begin{aligned} F_x &= -R_x \sin^3\theta/|\chi_{0r}|, \\ F_y &= -R_y \sin\theta/|\chi_{0r}|. \end{aligned} \tag{47}$$

This result is the same as in the papers by Hrdý & Siddons (1999) and Hrdý *et al.* (2001*b*) obtained on the basis of the usual plane-wave dynamical diffraction theory. It follows from (47) for a point focusing,

$$R_y = R_x \sin^2\theta. \tag{48}$$

7. Focus spot size and intensity

Let us consider the point focusing case [see the condition (48)]. At the distance $L_{hf} = L_{hfx} = L_{hfy}$ (on the point focusing plane) from (41) one obtains

$$I_h^{(e)} = \left|\tilde{E}_h^{(e)}\right|^2 = \left(\frac{S}{\lambda L_{hf}} \frac{\sin P_\xi}{P_\xi} \frac{\sin P_y}{P_y}\right)^2 \left|\bar{E}_{h1}\right|^2, \tag{49}$$

where $S = 4a_x|R_x|\sin^3\theta$ is the area of the integration region (in the plane perpendicular to the propagation direction of the reflected beam), $P_\xi = ka_x \sin\theta(\Delta\theta + \xi/L_{hf})$, $P_y = k|R_y|y/L_{hf}$. $\bar{E}_{h1}$ is the mean value of the diffracted wave amplitude on the entrance surface of the crystal inside the reflection region and $|\bar{E}_{h1}|^2 \simeq 1$. From (49) one can estimate the maximal value of the intensity at the focus point,

$$I_{max} = (S/\lambda L_{hf})^2 \left|\bar{E}_{h1}\right|^2. \tag{50}$$

The equation (49) allows the focus spot sizes $\Delta\xi_f$ and Δy_f to be estimated in the $O\xi$ and Oy directions, respectively. In particular, for the important case of an incident plane wave,

$$\Delta\xi_f = \frac{\lambda F}{a_x \sin\theta} = 2\lambda/\Delta\varphi_x \tag{51}$$

and

$$\Delta y_f = \frac{\lambda F}{|R_y|} = 2\lambda/\Delta\varphi_y. \tag{52}$$

Here, $F = F_x = F_y$ is the common focal distance when the condition (48) (point focusing) is fulfilled. The angles $\Delta\varphi_x = 2a_x \sin\theta/F \simeq \sqrt{2}\,2|\chi_{hr}|/\sin 2\theta$ (assuming $|\chi_{0r}| \simeq |\chi_{hr}|$) and $\Delta\varphi_y = 2|R_y|/F \simeq 2\cos\theta\,2|\chi_{hr}|/\sin 2\theta$ are the view point angles of the groove reflection region from the focus point in the (x, z) and (y, z) planes, respectively. These angles are approximately proportional to the angular width of the dynamical diffraction reflection curve for a crystal with a plane entrance surface. The formulae (51) or (52) are the same as for a curved mirror (Michette, 1986) if we replace angles $\Delta\varphi_x$ and $\Delta\varphi_y$ with the angular size of the specular reflection region proportional to $(|\chi_{0r}|/2)^{1/2}$, which in some order is larger than the dynamical diffraction reflection region. Thus, in the case of the same wavelength, the focus spot size for a mirror is smaller. However, the mirrors are used for soft X-ray focusing, which can have a significantly large wavelength.

8. Example

Let us consider the case of a Si(220) reflection, $\lambda = 0.71$ Å (17.46 keV) radiation, incident plane wave, σ-polarization, $|R_x| = 1$ mm, $|R_y| = |R_x|\sin^2\theta = 34$ µm (point focusing), $\Delta\theta = |\chi_{0r}|/\sin 2\theta$. According to (47), $F = F_x = F_y = 1.98$ m. In Fig. 3

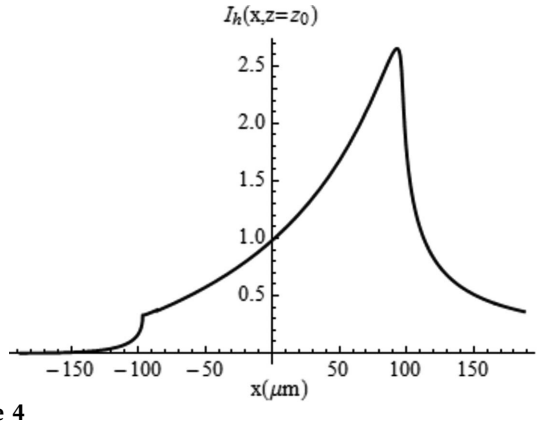

Figure 4
Intensity of the reflected wave on the entrance surface.

the dependence of the reflection region size $2a_x(L_s)$ [see (32)] is shown. For $L_s = 2F$, the reflection region size has maximum value $2a_x(2F) = 2|R_x|\tan\theta = 375$ μm. According to (32) the reflection region size for an incident plane wave $2a_x(L_s \to \infty) = 2a_x(F) = 193$ μm. In Fig. 4 the intensity distribution $I_h(x) = |E_h(x)|^2/|E_0^{(i)}|^2$ on the entrance surface in the region $-|R_x|\tan\theta < x < |R_x|\tan\theta$ is presented. In the reflection region -96.7 μm $\leq x \leq 96.7$ μm the intensity increases and has a maximum value at $x = a_x = 96.7$ μm. The behavior of the intensity significantly differs from the intensity behavior for a plane-entrance-surface perfect crystal. Despite this, the reflection coefficient $R(x)$ [see (37)] has the same behavior (Fig. 5) as for a plane-entrance-surface perfect crystal. Its behavior differs from the behavior of intensity. The difference between the behaviors of the intensity and reflection coefficient in our case is due to geometrically asymmetric reflection on both sides of the apex of the groove; meanwhile, for a curved mirror the reflection geometrically is symmetric in the whole reflection region. For a curved mirror the reflection coefficient and intensity have the same behavior. The behavior of the reflection coefficient shows that the whole reflected flux is less than for the incident beam (taking into account absorption), despite the fact that the intensity can be greater than unity (Fig. 4). But, as in our case as well as for a curved mirror, the absorption gives rise to an asymmetric reflection curve. In Fig. 6 using (41) the numerically calculated intensity

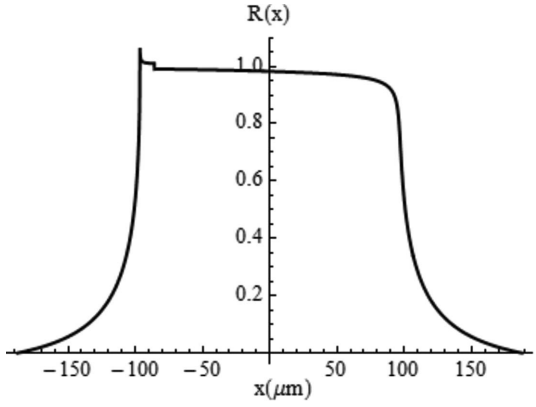

Figure 5
Reflection coefficient of the reflected wave.

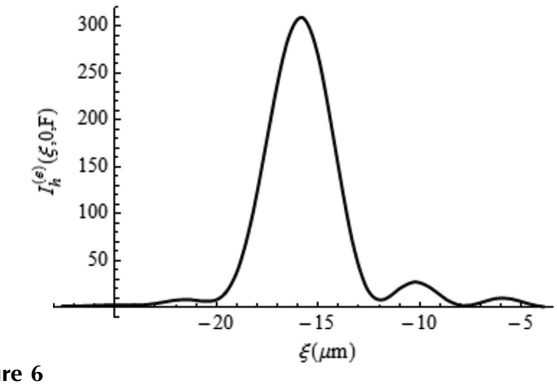

Figure 6
Intensity distribution of the reflected wave on ξ near the focus point on the focal plane, $y = y_f = 0$, $L_h = F$.

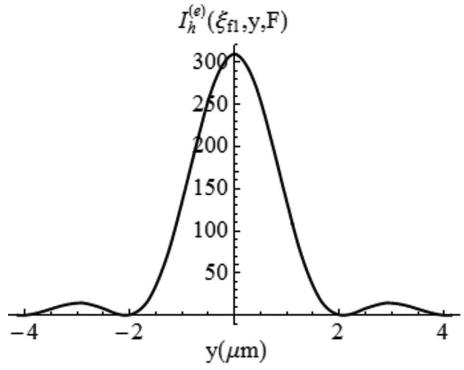

Figure 7
Intensity distribution of the reflected wave on y near the focus point on the focal plane, $\xi = \xi_{f1}$, $L_h = F$.

distribution $I_h^{(e)}(\xi, 0, F) = E_h^{(e)}|^2/|E_0^{(i)}|^2$ on ξ at the focal distance F in the plane $y = 0$ is shown. As can be seen, the intensity has a maximum at the point $\xi = \xi_{f1} = -15.8$ μm which slightly differs from the focus point coordinate $\xi_f = -17.3$ μm defined in (45). This difference is due to the phase of the reflected wave on the entrance surface of the crystal. For $\xi < \xi_{f1}$ the intensity is less than for $\xi > \xi_{f1}$. This coincides with the behavior of the amplitude of the reflected wave on the entrance surface of the crystal (Fig. 4). The numerically calculated intensity distribution on y, $I_h^{(e)}(\xi_{f1}, y, F) = |E_h^{(e)}|^2/|E_0^{(i)}|^2$, at the focal distance F for $\xi = \xi_{f1}$ is shown in Fig. 7. According to Figs. 6 and 7 the behavior of the intensity distribution coincides with theoretical predictions [formula (50)]. The focus spot's sizes predicted by (51) and (52), $\Delta\xi_f \simeq 8$ μm and $\Delta y_f \simeq 4$ μm, coincide with the numerically calculated focus spot's sizes presented in Figs. 6 and 7. According to (50) the intensity maximum value $I_{max} \simeq 10^3$ is overestimated but has almost the same order as the numerically obtained intensity maximum $I_{max} \simeq 309$ (see Figs. 6 and 7).

The crystal data are taken from Pinsker (1982).

9. Summary

In this work, on the basis of the eikonal approximation, Bragg-case X-ray focusing with a parabolic-shaped entrance-surface perfect crystal is considered theoretically. The expressions for

focal distances, intensity gain and focus spot size are obtained. The point focusing condition is found.

An example is considered. The focusing experimentally can be realised using X-ray synchrotron sources of radiation (particularly FELs). The Bragg-case lens can be a focusing element of an X-ray beamline or FEL.

The author is grateful to Dr J. Hrdý for discussion and support.

References

Artemiev, N., Hrdý, J., Peredkov, S., Artemev, A., Freund, A. & Tucoulou, R. (2001). *J. Synchrotron Rad.* **8**, 1207–1213.

Authier, A. (2001). *Dynamical Theory of X-ray Diffraction.* Oxford University Press.

Balyan, M. K. (2013*a*). *J. Contemp. Phys. (Armen. Acad. Sci.)*, **48**, 144–146.

Balyan, M. K. (2013*b*). *J. Contemp. Phys. (Armen. Acad. Sci.)*, **48**, 247–252.

Chukhovskii, F. N. & Shtolberg, A. A. (1970). *Phys. Status Solidi*, **41**, 815–825.

Courant, R. & Hilbert, D. (1966). *Methods of Mathematical Physics*, Vol. 2. New York: Interscience.

Grigoryan, A. H., Balyan, M. K. & Toneyan, A. H. (2010). *J. Synchrotron Rad.* **17**, 332–347.

Hrdý, J. (1998). *J. Synchrotron Rad.* **5**, 1206–1210.

Hrdý, J., Artemiev, N., Freund, A. K. & Quintana, J. (2001*a*). *Proc. SPIE*, **4501**, 88–98.

Hrdý, J., Hoszowska, J., Mocuta, C., Artemiev, N. & Freund, A. (2003). *J. Synchrotron Rad.* **10**, 233–235.

Hrdý, J. & Hrdá, J. (2000). *J. Synchrotron Rad.* **7**, 78–80.

Hrdý, J. & Siddons, D. P. (1999). *J. Synchrotron Rad.* **6**, 973–978.

Hrdý, J., Ziegler, E., Artemiev, N., Franc, F., Hrdá, J., Bigault, T. & Freund, A. K. (2001*b*). *J. Synchrotron Rad.* **8**, 1203–1206.

Kohn, V. G. (2007). *Crystallogr. Rep.* **52**, 598–603.

Michette, A. G. (1986). *Optical Systems for Soft X-rays.* New York: Plenum Press.

Pinsker, Z. G. (1982). *X-ray Crystallo-optics.* Moscow: Nauka (in Russian).

Smirnov, V. I. (1981). *Kurs Vysshey Matematiki*, Vol. 4, part 2. Moscow: Nauka (in Russian).

Solimeno, S., Crosignani, B. & Di Porto, P. (1986). *Guiding, Diffraction and Confinement of Optical Radiation.* New York: Academic Press.

Takagi, S. (1969). *J. Phys. Soc. Jpn*, **26**, 1239–1248.